REPORT DOCUMENTATION PAGE

Form Approved
OMB No. 0704-0188

1. REPORT DATE *(DD-MM-YYYY)*	2. REPORT TYPE	3. DATES COVERED *(From - To)*
27-09-2011	Journal Article	

4. TITLE AND SUBTITLE

Stability of Flame-Shock Coupling in Detonation Waves: ID Dynamics (Preprint)

5a. CONTRACT NUMBER

5b. GRANT NUMBER

5c. PROGRAM ELEMENT NUMBER

6. AUTHOR(S)
Lord K. Cole, Ann R. Karagozian, and Jean-Luc Cambier

5d. PROJECT NUMBER

5f. WORK UNIT NUMBER
23041057

7. PERFORMING ORGANIZATION NAME(S) AND ADDRESS(ES)

Air Force Research Laboratory (AFMC)
AFRL/RZSS
1 Ara Road
Edwards AFB CA 93524-7013

8. PERFORMING ORGANIZATION REPORT NUMBER

AFRL-RZ-ED-JA-2011-390

9. SPONSORING / MONITORING AGENCY NAME(S) AND ADDRESS(ES)

Air Force Research Laboratory (AFMC)
AFRL/RZS
5 Pollux Drive
Edwards AFB CA 93524-7048

10. SPONSOR/MONITOR'S ACRONYM(S)

11. SPONSOR/MONITOR'S NUMBER(S)
AFRL-RZ-ED-JA-2011-390

12. DISTRIBUTION / AVAILABILITY STATEMENT

Approved for public release; distribution unlimited (PA #11854).

13. SUPPLEMENTARY NOTES
For publication in Combustion Science & Technology.

14. ABSTRACT

The study of detonation waves dates back to the late 19th century, where Chapman and Jouguet modeled detonations as a shock wave supported by the heat release of the combustible material in an infinitely thin zone, where all chemistry and diffusive transport takes place. Later Zel'dovich, von Neumann, and Doring independently represented the detonation as a confluence of a shock wave moving at a detonation velocity, followed by a chemical reaction zone of finite length; this came to be known as the ZND model for a detonation wave. While the true structure of detonation waves inevitably calls for multidimensional effects, the simple 1D structure still provides a rich spectrum of dynamical features which are worthy of detailed exploration. This is especially important for the study of deflagration to detonation transitions and sustained oscillating or galloping detonations. For a spark-induced detonation, as the detonation decays towards the self-sustaining Chapman-Jouguet mode from an over-driven mode, one obtains a sequence of physical oscillations between the flame and shock front. The numerical analysis of this effect has been explored by Cambier, using highly-resolved numerical simulations, albeit with only a 2nd-order shock capturing scheme. Similar calculations of the dynamics of detonation oscillations, albeit with a reduced chemistry model, have been performed elsewhere. In the present study, we utilize high-order spatially accurate numerical methods in order to achieve grid convergence and to reduce or eliminate numerical diffusion effects while providing a detailed analysis of the nonlinear dynamics involved in resolving detonations with complex reaction kinetics. The dynamical characteristics and coupling of large and small length scale physics associated with detonation instabilities are explored in detail.

15. SUBJECT TERMS

16. SECURITY CLASSIFICATION OF:			17. LIMITATION OF ABSTRACT	18. NUMBER OF PAGES	19a. NAME OF RESPONSIBLE PERSON
					Dr. Jean-Luc J. Cambier
a. REPORT	b. ABSTRACT	c. THIS PAGE	SAR	26	19b. TELEPHONE NUMBER *(include area code)*
Unclassified	**Unclassified**	**Unclassified**			N/A

Stability of Flame-Shock Coupling in Detonation Waves: 1D Dynamics

Lord K. Cole, Ann R. Karagozian
University of California, Los Angeles
Los Angeles, California, USA

Jean-Luc Cambier
Air Force Research Laboratory, Spacecraft Branch
Edwards AFB, CA 93524 *

1 Introduction

The study of detonation waves dates back to the late 19th century, where Chapman [1] and Jouguet [2] modeled detonations as a shock wave supported by the heat release of the combustible material in an infinitely thin zone, where all chemistry and diffusive transport takes place. Later Zel'dovich [3], von Neumann [4], and Döring [5] independently represented the detonation as a confluence of a shock wave moving at a detonation velocity, followed by a chemical reaction zone of finite length; this came to be known as the ZND model for a detonation wave.

While the true structure of detonation waves inevitably calls for multi-dimensional effects, the simple 1D structure still provides a rich spectrum of dynamical features which are worthy of detailed exploration. This is especially important for the study of deflagration to detonation transitions [6] and sustained oscillating or galloping detonations [7, 8]. For a spark-induced detonation, as the detonation decays towards the self-sustaining Chapman-Jouguet mode from an over-driven mode, one obtains a sequence of physical oscillations between the flame and shock front. The numerical analysis of this effect has been explored by Cambier [9] using highly-resolved numerical simulations, albeit with only a 2^{nd}-order shock capturing scheme.

Similar calculations of the dynamics of detonation oscillations, albeit with a reduced chemistry model, have been performed elsewhere [10–12].

In the present study, we utilize high-order spatially accurate numerical methods in order to achieve grid convergence and to reduce or eliminate numerical diffusion effects while providing a detailed analysis of the non-linear dynamics involved in resolving detonations with complex reaction kinetics. The dynamical characteristics and coupling of large and small length scale physics associated with detonation instabilities is explored in detail.

2 Numerical Methodology

2.1 Governing Equation

Since we are interested in the dynamics associated with the inviscid problem, we solve the Euler equations for a multi-species, real gas with a chemical source term, as shown below:

$$\frac{\partial}{\partial t}\mathbf{Q} + \frac{\partial}{\partial x}\mathbf{F}(\mathbf{Q}) = \mathbf{S}(\mathbf{Q}) \tag{1}$$

where the vectors represented by $\mathbf{Q}, \mathbf{F}$, and $\mathbf{S}$ are, respectively:

$$\mathbf{Q} = \begin{pmatrix} \rho_s \\ \vdots \\ \rho u \\ \hat{E} \end{pmatrix}, \mathbf{F} = \begin{pmatrix} \rho_s u \\ \vdots \\ \rho u^2 + P \\ (\hat{E} + P)u \end{pmatrix}, \mathbf{S} = \begin{pmatrix} \omega_s \\ \vdots \\ 0 \\ \sum_s \omega_s e_{0s} \end{pmatrix} \tag{2}$$

The total mixture density is $\rho = \sum_s \rho_s$, with ρ_s the density of species s, and P and u represent pressure and velocity, respectively. The total energy $\hat{E}$ may be written as

$$\hat{E} = \int \rho c_v(T) dT + \frac{1}{2}\rho u^2 \tag{3}$$

where $c_v(T) = \sum_s \rho_s c_{vs}(T)/\rho$ is the mass-averaged specific heat at constant volume. Note that the total energy, Eq. (3), does not include the potential chemical energy of the mixture, given by $\sum_s \rho_s e_{0s}$, where e_{0s} is the formation energy of the s^{th} species. Therefore, the formation energy appears in Eq. (2) as a source term, to account for the exo- or endo-thermicity of the chemical reactions and guarantee energy conservation. This approach has been found preferable to including the formation energy in the definition of

the mixture's total energy – in which case no heat of formation term is added to the total energy, due to chemical reactions is necessary – as it can yield better accuracy at composition discontinuities. In the governing equation, Eq. (2), ω_s represents the net production rate of the s^{th} species:

$$\dot{\omega}_s = \sum_r \nu_{rs} k_{fr} \prod_j \rho_j^{\nu'_{rj}} - \sum_r \nu_{rs} k_{br} \prod_j \rho_j^{\nu''_{rj}} \tag{4}$$

$$\nu_{rs} = \nu''_{rs} - \nu'_{rs}$$

where ν''_{rk} and ν'_{rk} are the coefficients of s^{th} species in the r^{th} forward and backward reactions, respectively, and k_{fr} and k_{br} and the forward and backward chemical rates of the r^{th} reaction.

It is noted that some recent studies (eg. Romick et al [13]) suggest that the inclusion of physical diffusion in a detonation simulation is needed to reduce or eliminate the effects of numerical diffusion on resolution requirements and to generate more physically accurate instabilities. Without these physical dissipation mechanisms of diffusion or viscosity, the chemistry provides the only time and length scales, and the spectrum of dynamical features of the system can potentially include very high-frequency phenomena, especially if the chemical kinetics are very stiff. The extent to which these phenomena can be reproduced is at question here, since an attempt at reproducing the physical characteristics of the problem would require multi-dimensional calculations. Therefore, it is essential that we eliminate as much as possible the artificial scales of numerical dissipation in order to capture the chemically-induced dynamics. For this purpose, in addition to the use of high-order, low-dissipation numerical methods, we have placed a special emphasis on grid resolution until grid-independent results are obtained.

2.2 Numerical Scheme and Chemical Reaction Mechanism

In the present study, a 5^{th}-order accurate Monotonicity Preserving Scheme(MP5) as formulated by Suresh and Huynh [14] is principally used for high order interpolation of a system of governing equations. The MP schemes form a class of high-order accurate, shock-capturing numerical algorithms especially equipped for solving non-linear hyperbolic systems of conservation law equations. The MP5 scheme has a 5^{th} order accuracy in smooth regions of flow-field, while reducing to 1^{st} order at flow discontinuities, a necessary condition to avoid spurious oscillations. This makes MP schemes well suited for resolving flow-fields where shocks and flame fronts are present. The MP schemes interpolate the value of the conserved variables (listed in the

definiton of the **Q** vector) at the cell interface. The interface flux is then solved utilizing the Roe Flux (RF) [15] building block with the Harten, Lax, van Leer, and Einfeldt [16] entropy fix applied to the eigenvalues. The RF scheme is slightly more computationally expensive than one of its popular variants, Local Lax Friedrich (LLF), but is less dissipative, making it optimal for studying stability and resolving high-frequency wave structures. A 3^{rd}-order Total Variation Diminishing (TVD) Runge-Kutta time integration scheme is used in conjunction with MP5.

A fifth order spatially accurate Weighted Essentially Non-Oscillatory (WENO), scheme as formulated by Shu & Osher [17] was used in conguncction with the Advection-Diffusion-Reaction (ADER) scheme of Titerev & Toro [18] to form the spatially 5^{th} order accurate ADER-WENO5 or simply AW5 scheme. ADER schemes utilize the high order spatial derivatives calculated by the underlying scheme, e.g. WENO, to generate the temporal derivatives using Rosonov's procedure [19], for example, $\partial_t u = \lambda \partial_x u$, $\partial_{tt} u = \lambda \partial_{xx} u$, etc. With the high order temporal derivatives, a simple Taylor series expansion is performed to acquire a higher order temporally and spatially accurate scheme. Since the expensive Runge-Kutta time integration steps are no longer required, ADER-WENO is extremely efficient and well suited for parallel computation.

Since complex chemical reaction mechanisms are simulated, an operator splitting [20] approach is implemented to facilitate the efficient computation of the coupling with the chemical kinetics. The latter generally form a stiff system and for stability reasons, are computed with a point-implicit backwards Euler method. As in a previous study [9], the chemical kinetics of a diluted hydrogen-oxygen-nitrogen mixture were solved. The chemistry includes eight reacting species, H_2, O_2, H, O, OH, HO_2, H_2O_2, H_2O, and the non-reacting diluent N_2. Thirty eight elementary reactions are used in this mechanism and the backward rates are computed from equilibrium constants. For this chemical system of moderate size, the Gaussian elimination scheme is the optimal choice for solving the chemical kinetics implicitly.

It should be emphasized that the operator-splitting approach used here is not the only choice available to us. In fact, a more accurate coupling would be obtained by solving a fully-coupled system (convection and chemistry together) with an implicit Runge-Kutta method. However, the computational cost would increase at least 3-fold on an already challenging problem, even in 1D. Furthermore, we are mostly concerned with the reproduction of wave phenomena within a small distance, i.e. the induction length; our grid spacing is sufficiently small that the time step becomes dominated by the Courant-Friedrichs-Lewy (CFL) limitation rather than the significant evo-

lution of the chemical kinetics. Thus, we leave the comparison of coupling and time-stepping methods as a topic for future work.

2.3 Code Validation and Testing

In order to ensure that small scale features are properly captured and the leading shock of the detonation is properly resolved by the numerical scheme, a series of validation test were performed. The first case, as prescribed by Shu & Osher in [21] demonstrates how well a numerical scheme resolves a shock propagating through a entropy disturbance. Figure 1 shows an example of the spatial variation in density at a given instant of time for this problem. It is clear that the MP5 scheme is able to capture a range of different complex wave structures in the flow quite accurately. The second case, referred to as the blast-wave problem in [22], tests the ability of a numerical scheme to capture the interaction of strong shocks with shocks and expansion waves. Figure 2 similarly demonstrates that complex waves interactions are accurately captured with modest grid resolution. By comparison, the AW5 solution shown in 3 is slightly more diffusive. This is despite the fact that no Runge-Kutta time stepping is used in that case. Since both methods are formally 5^{th}-order accurate in smooth regions, the difference in quality of the solutions is due to the limiter. In the following, most of the results regarding the detonation dynamics will be obtained with the MP5 scheme, while the AW5 scheme is used to evaluate the influence of numerical accuracy. We should also emphasize that the results shown in Figures 1-3 do not use any artificial compression at the contact discontinuities (CD). Thus, the profile near $x \simeq 0.600$ in the blast-wave problem could be made much sharper; however, the non-linear procedure necessary for sharpening CDs may also artificially sharpen the gradients in acoustic and entropy waves and affect the dynamics within the induction region of a detonation; to guarantee the absence of numerical artifacts in the solution, no artificial compression is used in the computations.

In the present study, we have modeled the detailed kinetics of the simplest combustion system. Another approach, commonly chosen in fundamental studies of detonation dynamics, is a 1-step model, in which the entire chemistry is described by the evolution of a single progress variable that follows an exponential relaxation with a characteristic time-scale given by the induction delay. This progress variable is also associated with the fractional amount of heat released into the flow. In that model, the delay follows a simple exponential fit $\tau_i \simeq e^{E_a/T}$. The delay being essentially caused by the need for a sufficient amount of radicals from chain-branching reactions,

and the production of those being an endo-thermic process, the parameter E_a in this formulation is an averaged activation energy of the key radical-producing reactions. This is a reasonable approximation to the chemistry in that region, albeit within limits. We have used the detailed chemistry to compute and parametrize the induction delay as a function of initial temperature, and pressure (the mixture being held fixed to stoichiometric hydrogen-air). As shown in Figure 4, the delay does follow an exponential form $t_i \propto \alpha(P)e^{\beta(P)/T}$, as expected. The parameter β in this formulation is an averaged activation energy of the key radical-producing reactions. However, this approach yields unrealistic profiles of the post-shock region, since the heat release is gradual. A better description is obtained with the 2-step model [12], where the heat release is associated with a second progress variable, whose evolution can start only at the end of the induction delay, which now follows a linear time variation. While this allows a separation between the induction and heat release zones, this model fails in several ways. First, the heat release is assumed independent of temperature, which is unrealistic, as the flow heating accelerates the combustion; generally speaking, a stiff differential equation for the progress variable can be used to reproduce this non-linear effect, but the dynamics can be different from the real conditions. Second, when the flame is accelerated towards the shock, the two reaction zones (induction and flame) start to merge, even if species diffusion is neglected; the enforcing of two separate zones with a 2-step model modifies the dynamics of the strongly coupled shock-flame system. Thus, we have used a realistic chemical system in order to gain a better understanding of the true dynamics; the comparison with the results obtained with a simplified 2-step model would then allow us to correlate the results with specific features of the chemical kinetics.

3 Detonation Dynamical Phenomena

3.1 Ignition and Instabilities

Direct initiation of the 1D detonation in the study is obtained in a chamber filled with a stoichiometric mixture of H_2 and air (temperature 300 K and pressure 1 atm) by setting a region adjacent to an end-wall of the simulated shock tube at high pressure (40 atm) and temperature (1500 K), as a simulated spark. The direction initiation is preferable to a deflagration-to detonation transition (DDT), since the latter is much more sensitive to initial conditions and grid resolution, requires species diffusion, and a very long computational domain to reproduce both the DDT and the subsequent

evolution of the detonation. Nevertheless, even direct initiation is sensitive to initial conditions and resolution. The requirements to achieve detonation ignition with the MP5 scheme include a grid cell size of less than $\Delta x = 50$ μm and a distributed simulated spark region (of a length 0.25 to 0.5 cm) with sufficiently high presure. Figure 5(a) illustrates the pressure contours of a spark ignited mixture which does not achieve detonation, while Figure 5(b) illustrates contours of the same mixture and grid resolution with a higher spark pressure that achieves detonation. The initial spark conditions can be related to the minimum energy and kernel size for direct initiation [23]. Similar studies by He & Karagozian [24] indicate there are both pressure and temperature requirements for the spark. Once a satisfactory kernel/spark size and pressure were found, these initial conditions were kept for the remainder of the studies.

The succesful detonation initiation event proceeds in two phases; first, the gas in the spark region rapidly burns and increases the pressure to even larger values, in a nearly constant-volume combustion process. This high pressure generates a strong shock which propagates into the unburnt mixture, which itself is ignited after a time delay and rapidly burns, starting from the region closest to the spark. In a scenario described as the SWACER mechanism [28], the combustion wave overtakes the leading shock and the coalescence of the two fronts leads to extremely high peak pressures for a very short time. This event is easily identified in the trace of the peak pressure versus time, as shown in Figure 6, and is referred to hereafter as the "re-explosion" event (the first explosion taking place within the initial spark region). Two different grid sizes are used in Figures 6(a) & 6(b). A more detailed examination for the dynamics for these two different grid sizes are shown in Figures 7 & 8, as will be discussed below.

The high pressure of this second explosion event initiates another strong shock, followed after an an induction length (ℓ, in the reference frame of the shock) by the combustion zone. The flame is initially strongly coupled to the shock ($\ell \rightarrow 0$) and the wave is over-driven, i.e., its speed exceeds that of the Chapman-Jouget (CJ) detonation. As the degree of overdrive decays and the detonation approaches the CJ limit, instabilities begin to appear, as shown in 6(a) after 35 μs and 6(b) after 25 μs.

Because the re-explosion is clearly identified, we can use this feature to conduct a preliminary study of the effect of grid resolution. Thus, we examined the variation of the measured time delay to the second explosion t_{exp}, for given initial spark conditions. In this study, the uniform grid spacing Δx was varied from $1\mu m$ to $20\mu m$. Figure 9 illustrates how the time to re-explosion for both the MP5 and AW5 schemes varies with the grid res-

olution. The peak in t_{exp} for the MP5 scheme curve in Figure 9 occurs at approximately $7.5\mu m$, whereas it is slightly lower, at approximately $5\mu m$, for the AW5 scheme. Since the latter is more diffusive than MP5, this is not surprising that the curve exhibits a smoother profile. The most striking feature here is the non-monotonic behavior, i.e. the presence of a maximum time to explosition, which delineates two regimes. For grid resolutions Δx below this critical value, the simulation is in a "convectively" dominant regime where the combination of the numerical scheme and grid resolution is sufficient to mitigate the effects of numerical diffusion to the detonation formation. Both schemes produce similar values of t_{exp} for $\Delta x < 2\mu m$, but for this complex kinetics scheme, time convergence for t_{exp} may not be reached except for $\Delta x < 1\mu m$, consistent with Powers & Paolucci's findings [25]. For grid resolutions greater than the critical value in Figure 9, we enter the numerically dissipative regime where coupling of the fluid and kinetics is enhanced due to numerical diffusion of temperature and chemical concentrations.

Given this result, we conclude that the spacing should be less than 5 or 7.5 μm, depending on the numerical scheme. To obtain results truly independent of the numerical effects, we should have $\Delta x \to 0$, since the two methods converge – presumably, since we are of course unable to run such a calculation – towards a single value for t_{exp} in that limit. If we allow ourselves a given error level (say 5%), we can use a spacing of approximately 5 μm. In these studies of the detonation propagation and shock-flame coupling dynamics, most of the results were obtained for a spacing of $\Delta x = 2.5\mu$m, thus suggesting good accuracy. Nevertheless, the time to re-explosion is but one parameter that is affected by grid resolution, and calculations of the shock-flame instabilities were repeated for several grid spacings to confirm the accuracy of the results.

The present spark-ignited detonation simulations, utilizing the two high-order schemes mentioned above, demonstrate the appearance of different instability modes. Figure 6 illustrates the peak pressure of in the entire computational domain, for two different grid sizes. After the re-explosion, the detonation is strongly overdriven, as mentioned earlier; this is characterized as a rather smooth region in the peak pressure trace, between 10 and $25^{+}\mu$s, in the high-resolution case of Figure 6(b). Instabilities appear when the detonation becomes close to the CJ condition, starting with a small-amplitude, but high-frequency mode – hereafter referred to as "HF" For the low-resolution case, the transition to the high-frequency (HF) mode occurs at a time of the order of $30\,\mu s$,,shown in detail in Figure 7(a). For the high-resolution case, the transition occurs earlier, at $25\,\mu$s. Around 45

μs, ther is a gradual shift towards a lower frequency but high-amplitude mode – referred to here as "HA". This transition is gradual in the high-resolution case, with both modes coexisting during a period of time (betwen approximately 44 and 48 μs), as shown in more detail in Figure 8(b). In the low-resolution case of 8(a), however, the behavior is less gradual and more chaotic. Clearly, there are significant effects of the grid resolution on the dynamics of the instabilities; furthermore, the appearance of sharp features in the traces also suggests that special care must be exercised in avoiding numerical procedures which can arbitrarily sharpen gradients, as mentioned above. Furthermore, there are clear differences in the specific dynamical features of these instabilities, e.g., in the time of initiation of high frequency behavior and in the temporal waveforms of instabilities.

The nature of these features bears more quantitative exploration. A simple fast Fourier transform (FFT) can be used to find the spectral content of these two modes and verify their grid independence, as shown in Figure 10. The spectral content of the simulations is relatively insensitive to the grid spacing, as long as we are below the critical value for the start of numerical diffusion. For both HA instabilities near a frequency of approximately 0.35 MHz and HF instabilities near 2.3 MHz, there is relatively little difference in results for $\Delta x \leq 2.5 \mu m$. At very high frequencies, above 4 MHz, there is some grid dependency. Frequencies above 4 MHz are not seen at coarse resolutions, and the spectral content around 4.5 MHz is likely to be a harmonic of the strong 2.3 MHz signal. Note that since the instabilities develop for a finite time only, the sampling statistics of the FFT are limited. Using wavelet decomposition did not provide improvements in the signal-to-noise ratio.

These results confirm earlier findings [9] as well as more recent studies [10,11], which have shown that a detonation at the CJ limit has two distinct instability modes. The high frequency mode always appears first and marks the transition from a 'stable' CJ detonation. These fluctuations in key properties (e.g. species concentration, temperature, and pressure) of the fluid within the induction zone are described by Oran and Boris [26] as 'hot spots'. In the present study, we have found that these 'hot spots' contribute to an initial stage of the flame dynamics. In this regime, the induction length is very small ($\ell << \ell_{CJ}$), and acoustic waves generated by the perturbed chemistry are rapidly transmitted to the shock. Because there is a very limited amount of fluid that can participate in the fluctuation of the heat release, only low-amplitude perturbations of the CJ peak pressure appear. As these acoustic waves reach the leading shock and strengthen it, their frequency can be measured as that of the fluctuations of the peak pressure.

Eventually the average induction length continues to increase and a second mode can be seen, which directly couples the flame speed with the shock, resulting in fluctuations with lower frequency but much higher amplitude, as will be discussed below. While similar studies by Ng et al [27], observed stability limits of detonations using complex kinetics, were were able to further resolve the detonation with higher schemes and more points.

3.2 Simplified Model

A model for the induction zone can be constructed, as composed of a leading shock, a heated, post-shock medium(fluid), and a flame front, all of which are illustrated in Figure 11. A single period of the detonation oscillation can be described, in the rest-frame of the shock, as follows. Fluctuations at the flame front create an acoustic (pressure) disturbance, which travels at the acoustic wave speed, λ_{ac}, through the induction zone until it reaches the leading shock. Upon contact, the pressure fluctuation carried by the acoustic wave will accelerate the shock and therefore alter the post-shock conditions, thus creating an entropy disturbance (temperature fluctuation). This entropy disturbance will propagate back into the induction zone at the entropy wave speed, λ_{en}, toward the flame front. Upon contact with the flame, the entropy wave will create a new acoustic disturbance in the flame, and the cycle will repeat. Figure 11 illustrates this phenomenon, while the equations below quantify the entropy and acoustic wave speeds.

$$\lambda_{en}(x,t) = \left.\frac{dx}{dt}\right|_{en} = u_2(x,t) \tag{5}$$

$$\lambda_{ac}(x,t) = \left.\frac{dx}{dt}\right|_{ac} = c(x,t) - u_2(x,t) \tag{6}$$

where $u(x,t)$ is the fluid velocity, $c(x,t)$ is local speed of sound, $D(t)$ is the detonation velocity, and $u_2(x,t) = |u(x,t) - D(t)|$ is the post-shock fluid velocity in the detonation reference frame.

From the wave speeds, the period of the cycle, τ, can be expressed by

$$\tau = \int_{x_s - x_f}^{0} \frac{1}{\lambda_{ac}(x,t)} dx + \int_{0}^{x_s - x_f} \frac{1}{\lambda_{en}(x,t)} dx \tag{7}$$

where $x_s = (t - t_0) \cdot D(t)$ is the position of the shock and x_f is the position of the flame.

At a 0^{th}-order approximation, the fluid properties in the induction region, $Q_2(x,t)$, are assumed to weakly vary with time for a given half cycle,

$\frac{\partial Q_2(x,t)}{\partial t} \simeq 0$ & $\frac{\partial Q_2(x,t)}{\partial x} \simeq 0$. From this approximation, the period can be determined

$$\tau = \frac{\bar{\ell}}{c_{a\to b} + u_{a\to b} - \bar{D}_{a\to b}} + \frac{\bar{\ell}}{u_{b\to c} - \bar{D}_{b\to c}} \tag{8}$$

where $\bar{\ell}$ is the period averaged induction length, $a \to b$ is the fluid state at the acoustic wave half-cycle, $b \to c$ is the fluid state at the entropy wave half cycle, and u_α, c_α, and $\bar{D}_\alpha$ are the the fluid speed in the detonation reference frame, speed of sound, and average detonation speed for half-cycle α, respectively. The model for acoustic and entropy half cycles are illustrated in Figure 12, in correspondence to observed oscillations. From the period of the combined cycles, the frequency in oscillations of the peak pressure trace is $f = \tau^{-1}$

3.3 Discussion & Analysis

From the simplified model expressed in Eq. (8), data were extracted at different peak pressure cycles from the high frequency as well as high amplitude regime. Figure 13 illustrates the evolution of the induction zone temperature profile in the detonation reference frame for a given period of the high amplitude mode. Using the simulation induction zone data and the period from Eq. (8), the frequency $f \approx 310\,khz$ is estimated, which is in excellent agreement with that obtained from the spectral analysis ($310 \pm 40\,khz$) shown in Figure 10. Performing the same analysis on the high frequency mode, illustrated in Figure 14, the frequency $f \approx 2.08\,MHz$ is estimated, which is in good agreement with the spectral analysis ($2.29 \pm 0.4\,Mhz$) which is shown in Figure 10.

The 'hot spot', which appears in the high frequency mode temperature profiles, Figure 14, is of particular interest. It appears to inhibit the flames progress toward the flame front by pre-burning the fluid in the induction zone. This pre-ignition effect does not allow the flame to accelerate, and in the case of the high frequency mode the detonation is still strongly overdriven. The combination of the short induction length, due to the strong overdrive, and the inhibited flame lead to the high frequency and relatively low amplitude oscillations in the peak pressure trace.

In the high amplitude regime, Figure 13, the flame is unihibited by the presence of the 'hot spot', which allows it to propagate through the induction zone unmolested. A SWACER-like [28] mechanism appears to govern the high amplitude regime where in the flame is furthest from the leading shock, $\bar{\ell}_{max}$, it is uninhibited by the 'hot spot' and will burn the fluid

in the induction and accelerate toward the shock, releasing large amounts energy.

4 Conclusion & Remarks

The present studies indicate that it is possible to utilize a spatially high order accurate scheme with appropriate resolution of induction (approximately 100 points per induction half length) to explore preferred re-explosion and instability modes of a 1D finite rate complex kinetics detonation. Appropriate resolution of the unstable detonation with complex kinetics requires an examination of a number of parameters in addition to peak pressure, including dominant frequencies, time to re-explosion, and surely other phenomena as well. A simple model for the transmission of acoustic and entropy waves creating the different instability modes (high frequency, low amplitude or HF and low frequency, high amplitude or HA) replicates very well the dominant modes and appears to be a reasonable description for the mechanism by which the instabilities arise.

There are a number of open questions that remain in the exploration of unstable detonations with complex reaction kinetics. A comparison of results from the present studies with those using a simplified (e.g., two-step) model would help to ascertain the importance of the chemistry in such overdriven detonations. Comparison of results with reduced chemistry models for a lower overdrive is similarly important. The question of the required degree of grid resolultion is also relevant to these issues. These and other phenomena will be explored in future studies.

References

[1] Chapman, D. L., "On the Rate of Explosion in Gases", *Philos. Mag.*, Vol.47, 1899, 0pp. 90-104.

[2] Jouget, E., "On the Propagation of Chemical Reactions in Gases", *J. de Mathematiques Pures et Appliquees*, vol. 1, pp. 347-425 (1905), continued in vol.2, pp. 5-85 (1906)

[3] Zel'dovich, Ja, B., "On the Theory of the Propagation of Detonation in Gaseous Systems", *Zh. Eksp. Teor. Fiz.*, vol.10, 542-568 (1940)

[4] Von Neumann, J., "Theory of Detonation Waves", *Von Neumann, Collected Works*, vol. 6, 1942.

[5] Doering, W., "On Detonation Processes in Gases", *Ann. Phys.*, vol.43, 421-436 (1943)

[6] Shepherd, J. E. and Lee, J. H. S., "On the transition from deflagration to detonation", *Major Topics in Combustion*, Springer-Verlag, 1992, pp. 439-487.

[7] Bourlioux, A. and Majda, A.J., "Theoretical and Numerical Structure for Unstable Two-Dimensional Detonations", *Combust. and Flame*, vol. 90, 211-229 (1992)

[8] Hwang, P., Fedkiw, R., Merriman, B., Karagozian, A. R. and Osher, S. J., "Numerical Resolution of Pulsating Detonation Waves", *Comb. Theory & Modeling*, vol. 4(3), 217-240 (2000)

[9] Cambier, J.-L. "Development of Numerical Tools for Pulse Detonation Engine Studies", Flygtekniska Försökstantalten FFA TN 1996-50, Aero. Research Inst. of Sweden, 1996.

[10] G. J. Sharpe and S. A. E. G. Falle, "Numerical simulations of pulsating Detonations. I. Nonlinear stability of steady detonations", Combust. Theory Modell. vol. 4, 217 (2000)

[11] Y. Daimon and A. Matsuo, "Detailed features of one-dimensional detonations", *Phys. Fluids*, vol. 15, 112-122 (2003)

[12] Leung, C., Radulescu, M.I. and Sharpe, G.J., "Characteristics analysis of the one-dimensional pulsating dynamics of chain-branching detonations", *Phys. Fluids*, vol. 22, 126101 (2010).

[13] Romick, C.M., Aslam, T.D., Powers, J.M., "Verified Calculation of Nonlinear Dynamics of Viscous Detonations", 23^{rd} ICDERS, Irvine, CA, USA, July 28, 2011

[14] Suresh, A. and Huynh, H.T. "Accurate Monotonicity-Preserving Schemes with Runge-Kutta Time Stepping", *Journal of Computational Physics*, vol. 136, 83-99 (1997).

[15] Roe, P.L., "Approximate riemann Solvers, Parameter Vectors, and Difference Schemes", *Journal of Computational Physics*, vol. 43, pgs 357-372, 1981.

[16] Harten, A., Lax P.D. and van Leer B., "On upstream differencing and Godunov-type schemes for hyperbolic conservations laws", *SIAM Rev.*, vol. 25, 3562 (1983).

[17] Shu, C.-W., Osher, S., "Weightid Essentially Non-Oscillatory" ADD

[18] Titarev, V.A., Toro, E.F., "ADER: Arbitrary High Order Godunov Approach", *Journal of Computation Physics*, vol. 17, pgs 609-618 (2002).

[19] Rosonov, V.V., Zh. Vych. Matem. Mat. Fiz 1(2), pgs 267-279, 1961.

[20] Strikwerda, J.C. *Finite Difference Schemes and Partial Differential Equations*, Society for Industrial and Applied Mathematics, 1989.

[21] Shu, C.-W., Osher, S., "Efficient Implementation of essentially non-oscillitaroy shock-capturing schemes, II", *J. Comp. Phys.*, vol. 83, 32-78 (1989).

[22] Woodward, P., Colella, P., "The Numerical Simulation of Two-Dimensional Fluid Flow with Strong Shocks", *J. Comp. Phys.*, vol. 54, 115-173 (1984).

[23] J.H.S. Lee, "Initiation of Gaseous Detonation", *Ann. Rev. of Phys. Chem.*, vol. 28, 75-104, Oct. 1977, DOI: 10.1146/annurev.pc.28.100177.000451

[24] He, X., Karagozian, A.R., "Pulse-Detonation-Engine Simulations with Alternative Geometries and Reaction Kinetics", Journal of Propulsion and Power, vol. 22, 852-861 (2006).

[25] Powers, J.M., Paolucci, S., "Accurate Spatial Resolution Estimates for Reactive Supersonic Flow with Detailed Chemistry", *AIAA*, vol 43, 1088-1099, May 2005.

[26] Oran, E.S. and Boris, J.P. *Numerical Simulation of Reactive Flow*, Elsevier Science, 1987.

[27] Ng, H.D., Nikiforakis, N., Lee, J.H.S, "The Suitability of a High Resolution Centered Scheme for Detonations Simulations", *Journal of Scientic Computing*, SIAM, submitted 2002.

[28] Lee, J.H., Knystaustas, R., Yoshikawa, N., "Photochemical initiation of gaseous detonations", *Acta Astronautica*, vol. 5, 971-982 (1978).

[29] Radulescu, M.I., Ng, H.D., Lee, J.H.S., Varatharajan, B., "The Effects of Argon Dilution on the Stability of Acetylene/Oxygen Detonations", *Proceedings of the Combustion Institute*, vol. 29, 2825-2831 (2002)

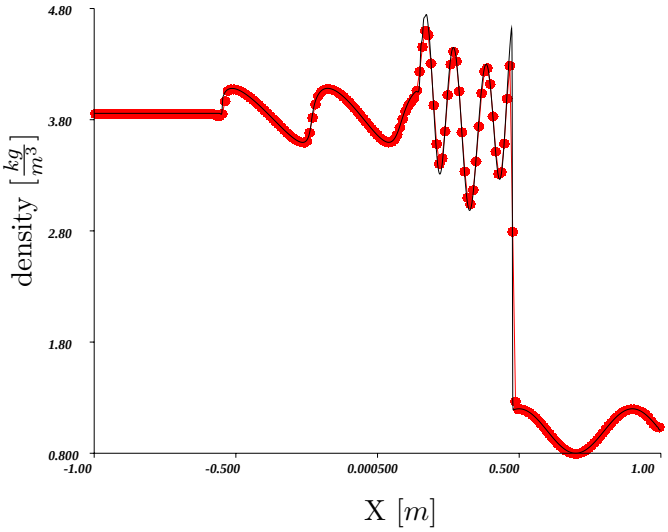

Figure 1: Computed (symbols) and exact solutio of density profile in Shu-Osher test problem at a given time. The MP5 scheme is used here.

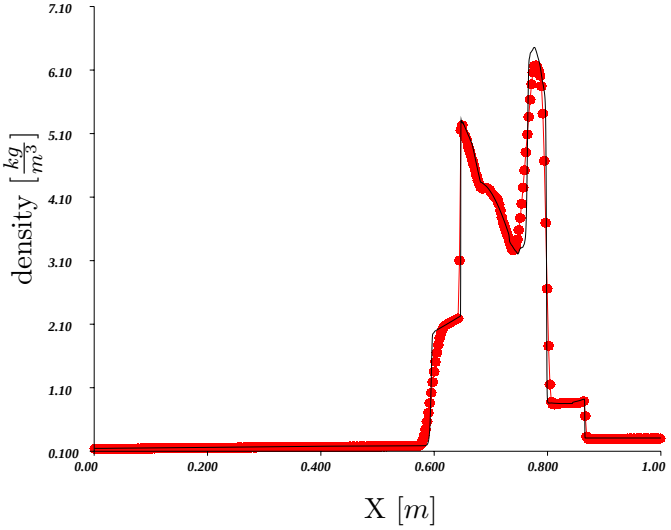

Figure 2: Computed (symbols) and exact solution of density profile in Blast-Wave test problem at a given time. The MP5 scheme is used here.

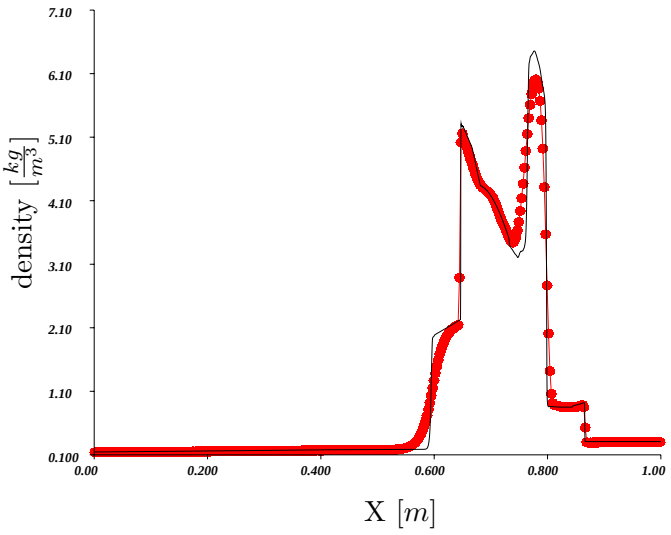

Figure 3: Computed (symbols) and exact solution of density profile in Blast-Wave test problem at a given time. The AW5 scheme is used here.

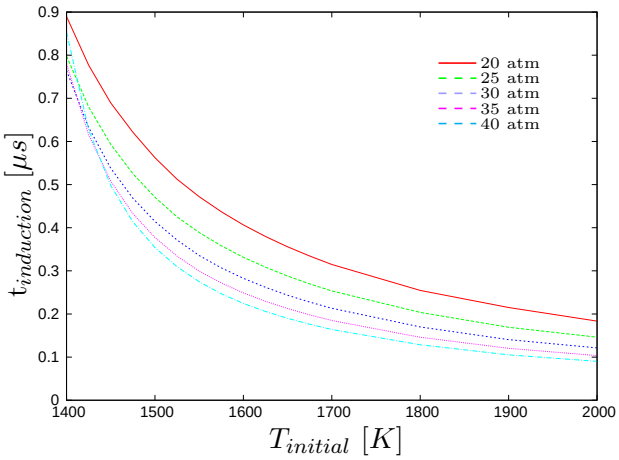

Figure 4: Induction Delay versus initial temperature for various pressures. Curves can be fitted as $t \sim \alpha(P)e^{\frac{\beta(P)}{T}}$

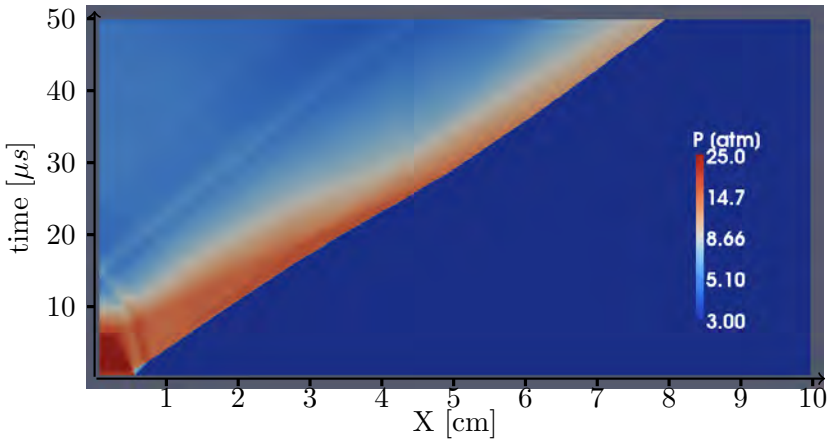

(a) $P_{spark} = 20atm$ with $0.25cm$ spark length where detonation is not achieved

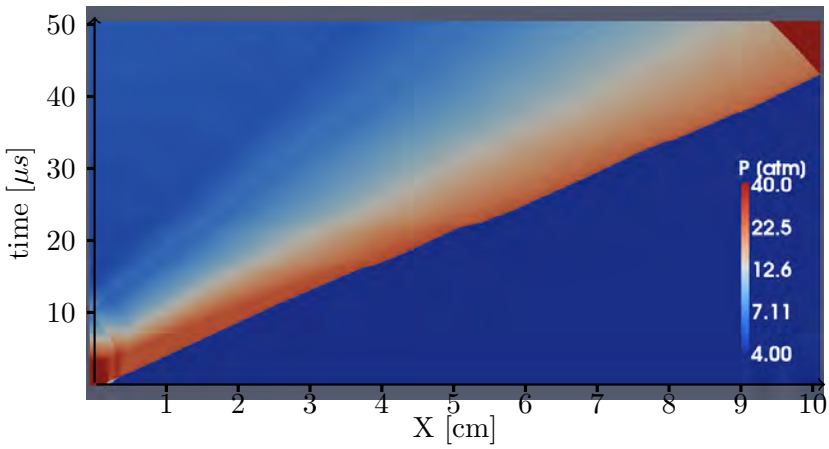

(b) $P_{spark} = 50atm$ with $0.5cm$ spark length where detonation is achieved

Figure 5: Pressure contour of a spark ignited H_2-Air mixture with $\Delta x = 50\mu m$.

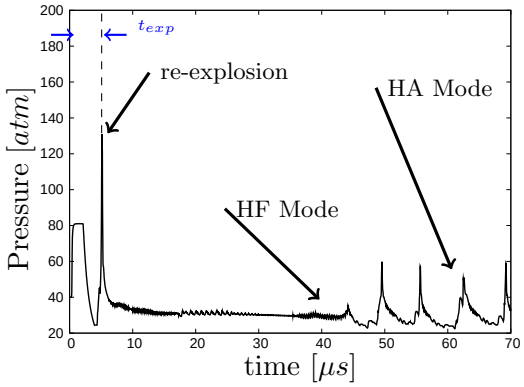

(a) $\Delta x = 12.5\ \mu m$

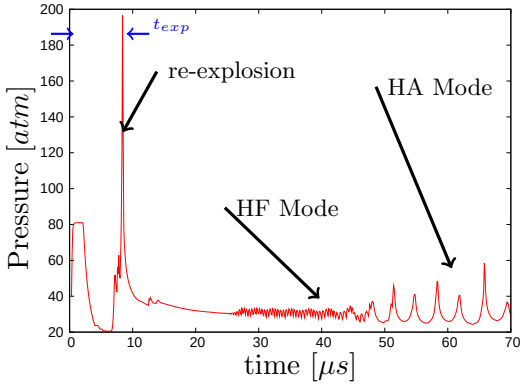

(b) $\Delta x = 2.5\ \mu m$

Figure 6: Peak pressure time history of a spark-ignited H_2-air mixture simulated with two different grid cell sizes Δx. The time to re-explosion, t_{exp}, high amplitude mode, HA, and high frequency mode, HF, are illustrated.

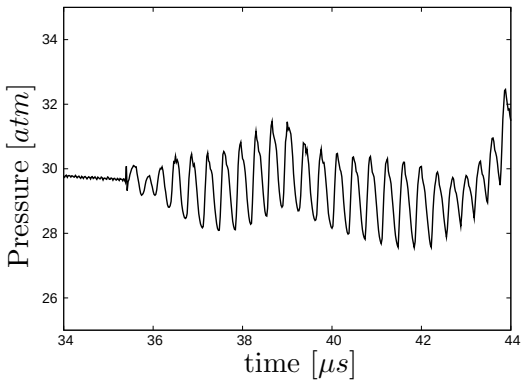

(a) $\Delta x = 12.5\ \mu m$

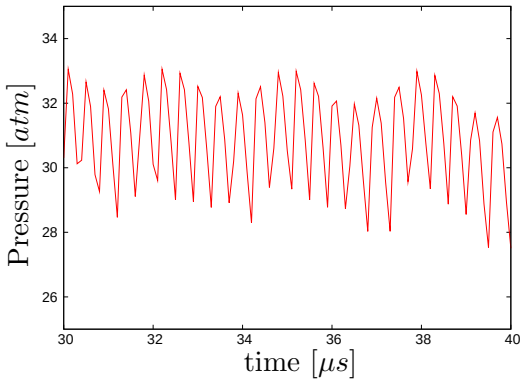

(b) $\Delta x = 2.5\ \mu m$

Figure 7: High frequency portion of peak pressure time history as in Fig. 6, simulated with two different grid cell sizes Δx.

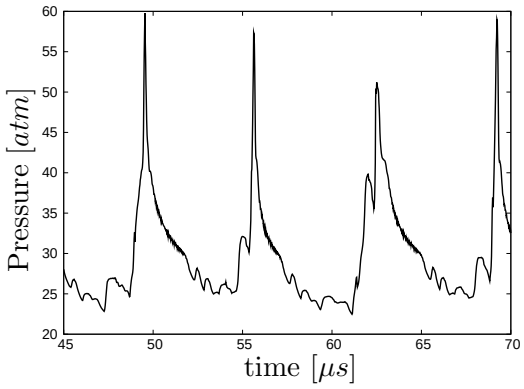

(a) $\Delta x = 12.5\ \mu m$

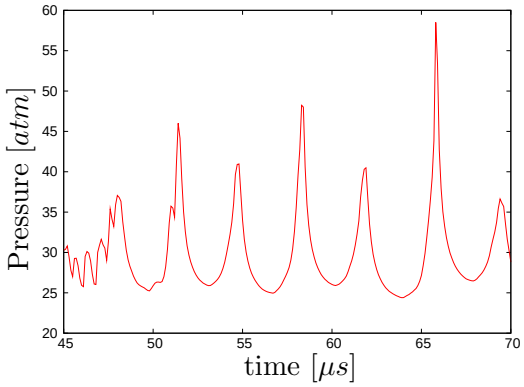

(b) $\Delta x = 2.5\ \mu m$

Figure 8: High amplitude portion of peak pressure time history as in Fig. 6, simulated with two different grid cell sizes Δx.

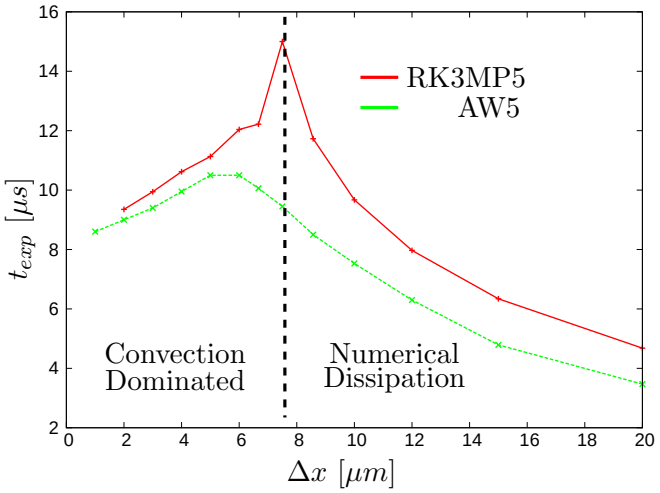

Figure 9: Time to re-explosion versus grid resolution for both MP5 (with 3^{rd} order Runge-Kutta) and AW5 schemes.

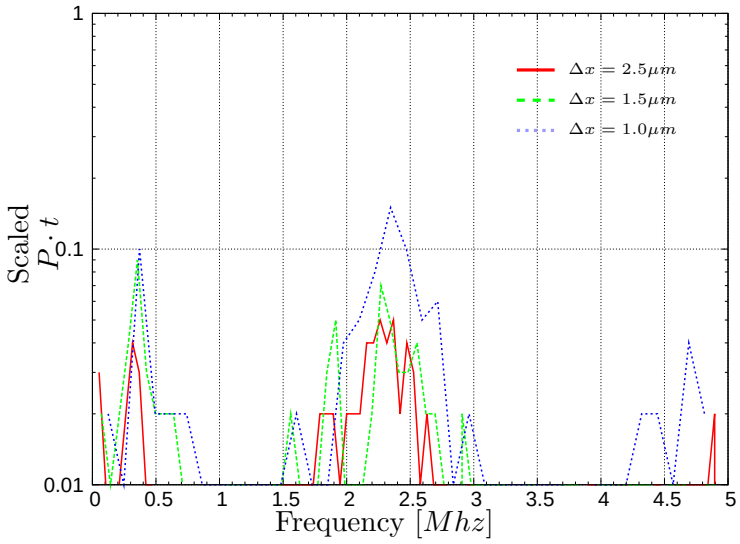

Figure 10: Fourier transform of peak pressure traces for the unstable detonation with 3 different sizes of Δx.

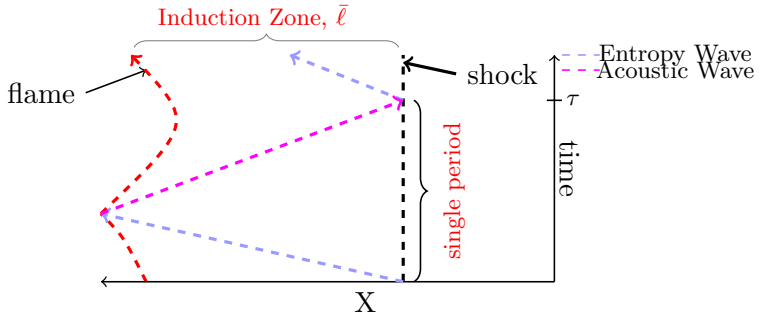

Figure 11: Model of shock, flame, induction zone, and transmission of entropy and acoustic waves for shock-flame coupling.

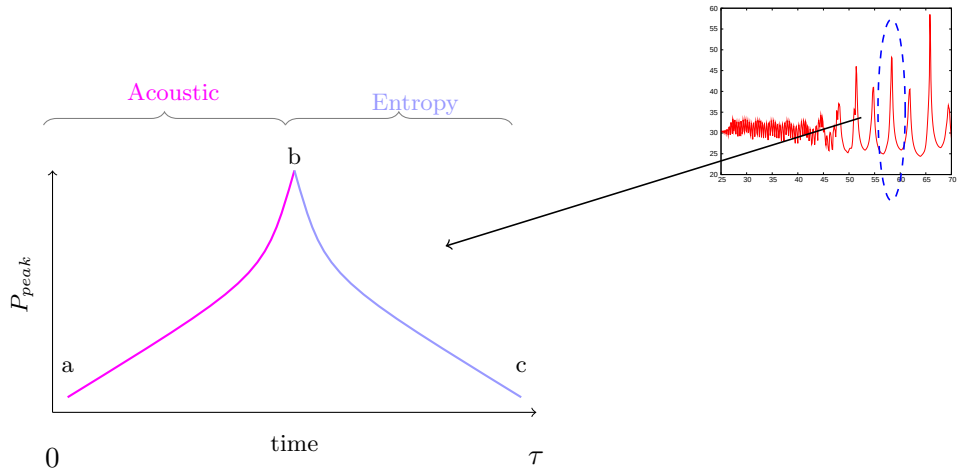

Figure 12: Simplified peak pressure cycle(left) used to represent the numerically observed pulsations in peak pressure(right).

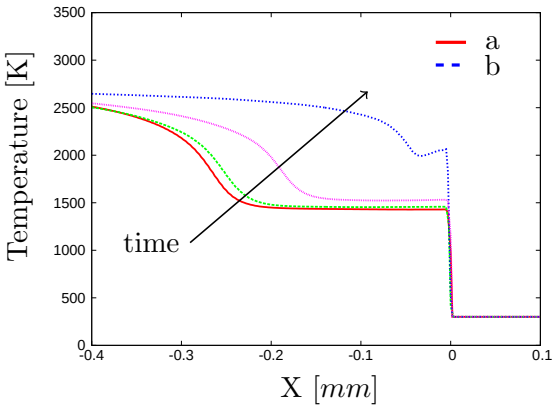

(a) acoustic wave cycle

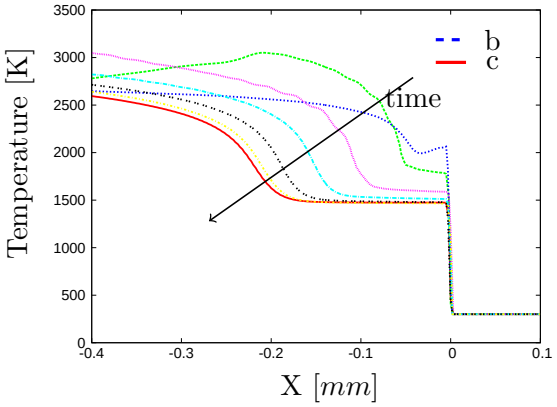

(b) entropy wave cycle

Figure 13: Temperature distribution in shock reference frame at different times within the acoustic wave (a) and entropy wave (b) cycle. Data is extracted from high amplitude mode results.

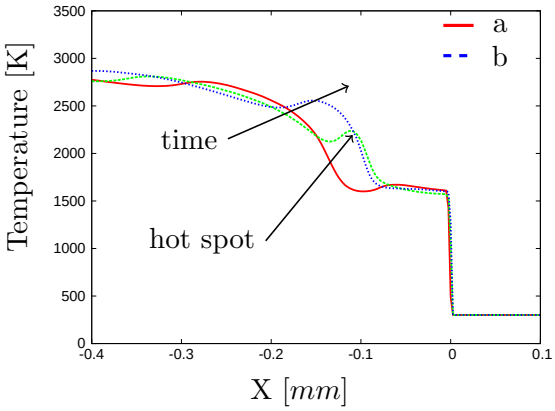

(a) acoustic wave cycle

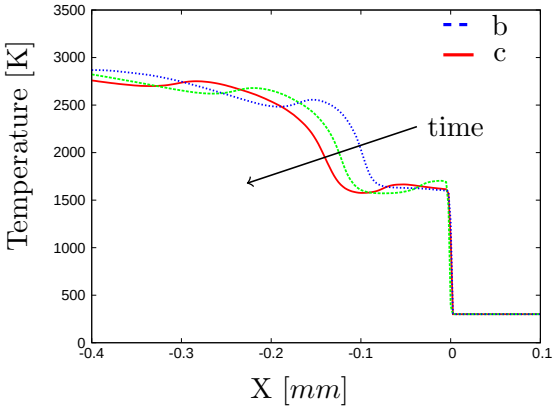

(b) entropy wave cycle

Figure 14: Temperature distribution in shock reference frame at different times within the entropy wave (a) and acoustic wave (b) cycle. Data is extracted from high frequency mode results.